10th ANKARA INTERNATIONAL AEROSPACE CONFERENCE **AIAC-2019-012**
18-20 September 2019 - METU, Ankara TURKEY

A COMPUTATIONAL STUDY ON ROTOR-PROPELLER ARM INTERACTION IN HOVERING FLIGHT

Serkan Yener[1]
Middle East Technical University
Ankara, Turkey

Mustafa Perçin[2]
Middle East Technical University
Ankara, Turkey

ABSTRACT

This paper presents a computational study on the interaction between rotor and propeller arm by using commercially available computational fluid dynamics (CFD) solver software ANSYS Inc. Fluent 17. Numerical results are validated for hovering and vertical climb flight conditions with force and torque measurements conducted on a 16inch propeller. Four different arm geometries are created and added to the validated CFD model to assess their effect on the aerodynamic performance of the propellers. The results of this study reveal that the propeller-Eppler arm configuration has 4.89%, 21.59%, and 5.18% greater propeller efficiency than that of the propeller-cylindrical arm, propeller-square arm, and propeller-slotted square arm configurations, respectively.

INTRODUCTION

Unmanned Aerial Vehicles (UAV) has become a rapidly growing aviation discipline in the field of military and civil aviation. In addition to being hobby items in the form of remote controlled (RC) airplanes, UAVs are designed to carry small payloads and are mainly used for surveillance and research needs [Deters, Ananda, & Selig, 2014].

[Brandt & Selig, 2011] pointed out the importance of propeller performance at low Reynolds numbers for designing and performance analysis of UAVs. They made wind tunnel measurements for 79 propellers which are used on small UAVs and model aircraft at the University of Illinois at Urbana-Champaign. The study proposes that the operation range of Reynolds number affects the overall aircraft performance. [Deters, Ananda, & Selig, 2014] extended the study by experimenting with 70 propellers, four of which were manufactured with a 3D printer. Their investigation intended to explore the influence of low Reynolds numbers on the performance of small-scale propellers. Accordingly, it is necessary to study the propeller performance and various other components of UAVs at low Reynolds numbers.

[Stajuda, Karczewski, Obidowski, & Krzysztof, 2016] emphasized the need for experimental research for the theoretical development in the field of propeller design. They stated that Blade Element Theory (BET) and Blade Element Momentum Theory (BEMT) could be used

[1] Graduate student in Aerospace Engineering Department, Email: srknyener@gmail.com
[2] Assistant Professor in Aerospace Engineering Department, Email: mpercin@metu.edu.tr

to assess the aerodynamic performance of the propellers. However, these methods require some experimental data for the sake of validation.

[Kutty, Rajendran, & Mule, 2017] proposed a numerical prediction method to determine APC Slow Flyer propeller performance under low Reynolds number conditions by using CFD. Their CFD results agreed well with the experimental results obtained by [Brandt & Selig, 2011] and thus, CFD can be a reliable analyzing method for propeller performance studies.

Rotor-rotor and rotor-airframe aerodynamic interactions are essential parameters in the performance of small scale UAVs. [Theys, Dimitriadis, Hendrick, & Schutter, 2016] investigated the influence of the propeller configuration, shape, and dimension of the propeller arm on the rotor aerodynamic performance experimentally. Three different type of arm shapes (cylinder, square, and aerodynamic geometry) were tested, and they showed that the square shape was the best design due to having the better propulsion system efficiency in hovering flight.

[Penkov & Aleksandrov, 2017] performed experiments and numerical analysis to investigate rotor-rotor interactions, and they compared the results from experiments and CFD simulations. Eventually, they came up to an optimal distance between rotors. Evidently, CFD simulations are employed to understand rotor-rotor and rotor-airframe aerodynamic interactions better. In addition to this, new designs can be evaluated accurately in any situation in a less time-consuming way.

The objective of this study is to investigate the interaction between propellers and rotor frame arm of different geometries in hovering flight and to assess the influence of the frame arm on the aerodynamic performance of the rotor. In the first step, simultaneous torque and thrust measurements were made for a 16-inch propeller, and the results were compared with the numerical simulations performed in ANSYS Fluent. In the second step, four different arm shapes were included in the numerical flow solutions for the 16-inch propeller in order to assess their influence on the aerodynamic rotor performance.

METHOD

Models

In this study, two different propellers were used. The first one, APC Slow Flyer 11x4.7 propeller, is used for the validation of the experimental setup that is utilized for thrust and torque measurements. The measured thrust and torque values at different RPM settings both in hovering and vertical climb flight configurations were compared to the experimental data reported by [Brandt & Selig, 2011]. The second one, 16x4 carbon fiber propeller, is the primary experimental model used in this study.

Four different arm shapes were designed to investigate rotor-propeller arm interaction. These are Eppler Arm, 25mm cylindrical tube, 25mm square tube and 25mm square tube with a 10mm slot. Eppler Arm is the arm with E 862 Airfoil, which was designed especially for non-lifting struts by Richard Eppler [Eppler, 1990]. The airfoil is scaled to have a maximum thickness of 25 mm. In the last step, torque and thrust values from the four cases in hovering flight were compared with each other. The schematics of arm propeller configurations are shown in Figure 1.

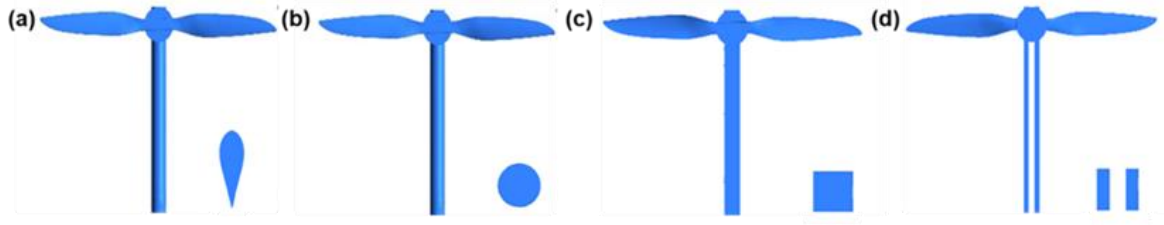

Figure 1: (a) Eppler Arm, (b) Cylinder Arm, (c) Square Arm, (d) Slotted Square Arm

Experimental setup

Thrust and torque measurements were conducted in a low-speed suction type METU Rüzgem wind tunnel which is powered by a 45-kW speed controlled electrical motor. The wind tunnel contains a 2D contraction section with an area ratio of 1:5. The free stream velocity was measured with a portable hot wire anemometer. A Quanum MT Series 4108 370KV brushless multirotor motor, an ATI Gamma load cell and the propeller were mounted to a mechanical structure which was designed and manufactured by [Kaya, 2014]. Then, the whole structure was placed in the test section of the wind tunnel. The ATI Multi-Axis Force/Torque Sensor system measures all six components of force and torque

Angular velocity of the propellers was adjusted with an optical RPM sensor. Thrust and torque measurements were performed at the data acquisition frequency of 1000 Hz. Ambient pressure and temperature were also recorded during each run. Each test is repeated three times for both propellers and flight conditions. The measurement matrix is tabulated below in Table 1.

Table 1. Thrust and torque measurement conditions

	Hovering Flight	Vertical climb Flight	
Propeller Type	Rotational speed of the propeller (RPM)	Rotational speed of the propeller (RPM)	Free Stream Velocity (m/s)
APC Slow Flyer 11x4.7	2556, 3423, 4290 and 5175	3004 and 4003	4.91, 6.14 and 8.03
Carbon Fiber 16x4	1050, 2000 and 3150	2000 and 3150	3.42 and 5.42

As a result of the hovering flight test comparison study, when compared with the relevant experimental data of Brandt, a maximum discrepancy of 5.65% for thrust coefficient and 5.97% for power coefficient was obtained.

As a result of the advancing flight test comparison between two studies, a maximum inconsistency of 8.46% for the thrust coefficient and 6.08% for the power coefficient was obtained. Investigation proved that the applied testing method was reliable for other conducted tests of the current study. Thus, a proper comparison for experimental and numerical analysis for 16-inch carbon fiber propeller is possible.

Numerical setup

Commercially available CFD solver ANSYS Inc. Fluent 17 is used for numerical solutions. The Multiple Reference Frame model (MRF) approach is applied to analyze the flow around the 16-inch propeller. CFD simulations were conducted in both advancing and static flow conditions at various rotational speeds and free-stream velocities. An interface is used to transfer flow data to the adjacent domain zones. Reynolds-Averaged Navier-Stokes (RANS) simulations were performed by implementing the k-ω turbulence model.

Flow domain and boundary conditions were demonstrated in Figure 2a. The domain consists of a rotating domain in which the propeller is surrounded by a cylinder and a stationary domain. Only half of the physical domain was computed in propeller-only simulations as a two-bladed propeller was analyzed, which allows for a rotational periodicity. For the arm structure investigation part, on the other hand, the complete physical domain is simulated. The 16-inch propeller is placed in the center of the rotational domain, as shown in Figure2b.

Height of the stationary domain is 8 times the diameter of the propeller. For the rotating domain that is located at the center of the stationary domain, the cylinder enclosure is set to be 1.1D and 0.4D.

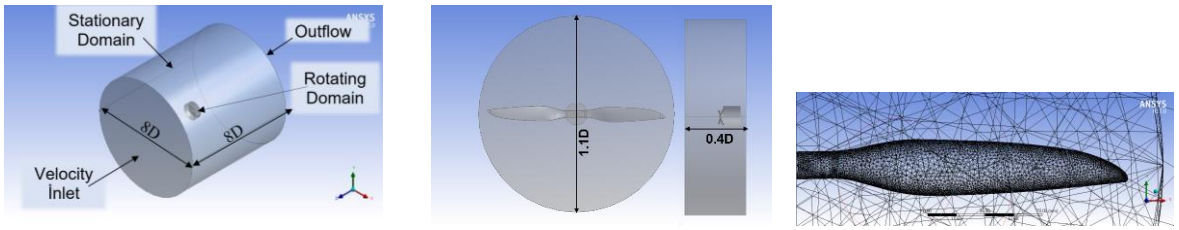

(a) (b) (c)

Figure 2: (a) Flow domain and boundary conditions, (b) Rotating domain, (c) Surface mesh of propeller

The mesh for the study was generated using the mesh generation tool in Ansys Fluent 17.0. The mesh is unstructured and composed of tetrahedral elements in both domains. A high-quality computational grid is crucial to provide reliable results and to solve the boundary layer on the propeller surface fully. A portion of the mesh along the propeller blade surface is shown in Figure 2c.

Mesh independence analysis was performed, and the case of 1.5 x 10^6 cells was found to be the optimal case for both hovering and vertical climb flight conditions.

Model independence analyses were done with different turbulence models for both hovering and vertical climb flight conditions. Although a similar trend was observed with all of the considered turbulence models, the k-ω turbulence model yielded the most accurate results, so it was selected to be used in the subsequent numerical solutions.

RESULTS AND DISCUSSION

In this section, the 16-inch carbon propeller test and CFD results will be presented and discussed. First, thrust and torque measurement results will be compared with the numerical simulations performed in ANSYS Fluent. Then, the interaction between propellers and rotor frame arm of different geometries and the influence of the frame arm distance to the propeller on the aerodynamic performance of the rotor in hovering flight will be described.

Carbon Fiber 16x4 propeller test and CFD results

Figure 3 and Figure 4 show the comparisons of the Carbon Fiber 16x4 propeller hovering and vertical climb flight performance results obtained from CFD simulations and tests. Hovering flight thrust and torque values versus the corresponding RPMs are shown in Figure 3. Thrust and power coefficients versus the corresponding advance ratio values are shown in Figure 4 for vertical climb flight.

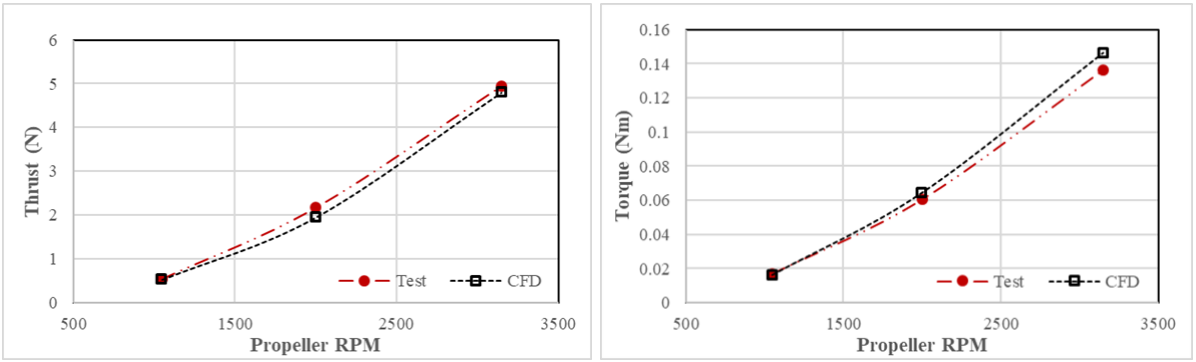

Figure 3. Comparison of the thrust and torque data obtained from CFD simulations and measurements for the Carbon Fiber 16x4 propeller in hovering flight

As a result of the hovering flight CFD simulation comparison study, when compared with the relevant test data, a maximum discrepancy of 10.44% for the thrust and 7.28% for the torque value is obtained. The average error value achieved from the test results comparison data is 5.79% for the thrust and 6.19% for the torque values.
As a result of the vertical climb flight CFD simulation comparison study, a maximum inconsistency of 10.81% for the thrust coefficient and 4.06% for the power coefficient is obtained when compared with the relevant test data. The average error value achieved from the test results comparison data is 4.78% for the thrust coefficient and 2.18 % for the power coefficient. Thus, the comparative analysis has proven that the CFD method is reliable for other similar CFD studies.

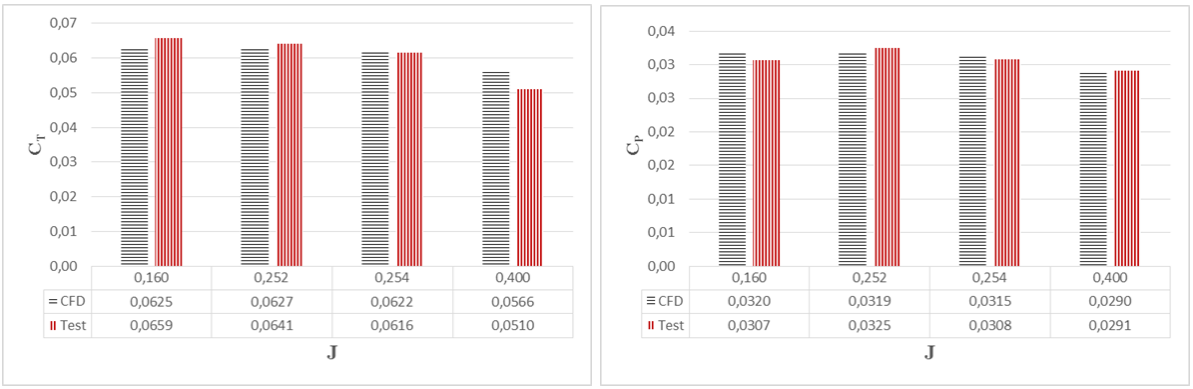

Figure 4. Comparison of the thrust and power coefficient obtained from CFD simulations and measurements for the Carbon Fiber 16x4 propeller for vertical climb flight

Since some errors were observed in comparison of the test results for APC Slow Flyer 11x4.7 propeller between METU and UIUC tests, the majority amount of differences in the comparison of the CFD and the test results of carbon fiber 16x4 propeller can be considered due to some errors in the experimental measurements.

The force and moment around the propeller three-coordinate system describe the thrust and torque, respectively. Thrust coefficient,C_T, power coefficient,C_P, and advance ratio,J, are defined in by Equations (1)-(5). Air density is calculated according to the equation of state (1).

$$\rho = \frac{\mathrm{P}_{atm}}{\mathrm{R}T_{air}} \quad (1)$$

$$P = 2\pi nQ \quad (2)$$

The propeller power can be calculated from Equation 2. Propeller measurements and calculations are non-dimensionalized to acquire the performance data. The power and thrust coefficient equations are shown below (Equation 3 and Equation 4).

$$C_P = \frac{P}{\rho n^3 D^5} \quad (3)$$

$$C_T = \frac{T}{\rho n^2 D^4} \quad (4)$$

$$J = \frac{V}{nD} \quad (5)$$

In hovering flight condition, the efficiency of the propeller η_{prop} is calculated using momentum theory as defined by [Theys, Dimitriadis, Hendrick, & Schutter, 2016]. The efficiency of the propeller η_{prop} is described by Equations (6)-(10).

In these equations, T (N) is the thrust produced by propeller, Q (Nm) is torque, ρ (kg/m3) is the density of the fluid, V (m/s) is the airspeed ahead of the propeller, V_1 is the airspeed at the propeller disk and v_i is the induced velocity, D (m) is the diameter of the propeller and n (rps) is the rotational speed of the propeller, ω (rad/s) is the angular speed of the propeller, A (m^2) is the disk area of the propeller. For advancing flight conditions, the advance ratio can be described as the ratio of velocity and the rotation rate (Equation 5). For hovering flight conditions, J becomes zero (because of V =0). The propeller efficiency (η_{prop}) is identified as the ratio between the induced power (P_i) and the required mechanical power (P_{mech}).

$$V = 0 \tag{6}$$

$$V_1 = v_i \tag{7}$$

$$T = 2\rho A(v_i)^2 \tag{8}$$

$$P_i = TV_1 \tag{9}$$

$$\eta_{prop} = \frac{P_i}{P_{mech}} = \frac{T^{\left(\frac{3}{2}\right)}}{Q\omega\sqrt{2\rho A}} \tag{10}$$

Rotor frame-arm interaction study results

Prominent pressure contours of the rotor frame-arm of four different geometries will be examined to investigate the main features of the flow field. The rotor frame-arm simulations were considered for hovering flight configuration. The contours are shown at the center plane (y-z plane) of the arm. The interaction study was conducted with three different rotor frame-arm distance (i.e., small, middle, and long-distance). First, consistency of the MRF approach in itself for rotor-propeller arm interaction study will be examined. Afterwards, the pressure contours of the small distance square-frame arm configuration will be explored to examine whether the presence of the arm has any effect on performance. Then, small distance frame-arm configuration performance comparison between the four different frame-arm will be explained. Finally, pressure contours of the small, middle, and long-distance frame-arm configurations will be evaluated for the Eppler frame-arm and the slotted square frame-arm, respectively.

Examining the consistency of MRF approach in itself

For the arm structure study, six new rotating domains were created to check the consistency of the MRF approach in itself. In order to achieve this, the propeller was rotated six times with 30-degree intervals. In Figure 5, the comparison of the thrust coefficients with and without the presence of the rotor-frame arm shapes are shown with respect to the different propeller phase angles. According to the results, although the propeller position is different, similar trends are observed for the 12 propeller positions.

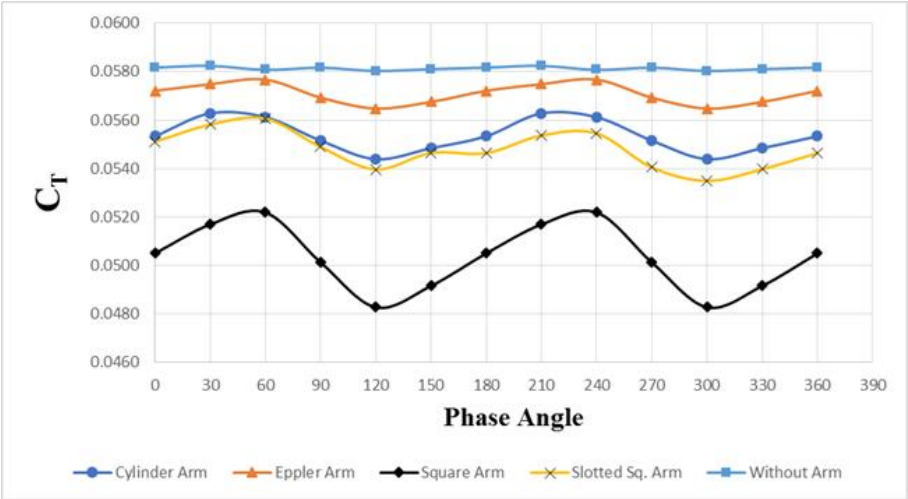

Figure 5. Comparison of the thrust coefficients obtained from CFD simulations for the different arm shapes with respect to the different propeller phase angles

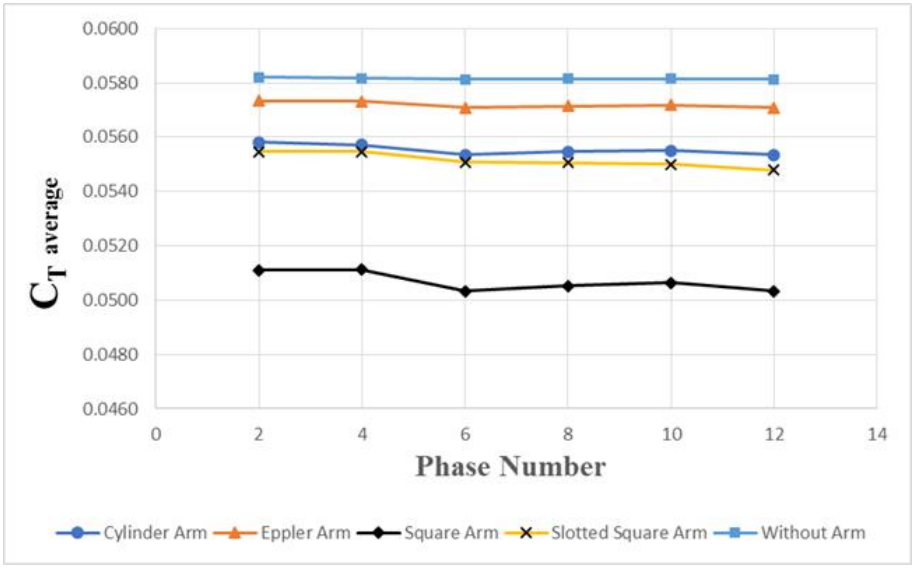

Figure 6. Comparison of the thrust coefficient averages for the different arm shapes with respect to the different propeller phase numbers

The thrust coefficient results which are obtained from the different propeller phases (see Figure 5) are averaged to examine the phase number effect. Figure 6 presents the comparison of the averaged thrust coefficients versus the phase number for with and without the presence of the rotor-frame arm shapes. As shown in the figure, the average thrust coefficient results are approximately the same as the number of phase increases. The simulation results in different phase angles have yielded similar results for all arm types. As a result of this study, it can be said that the angle that the rotor is positioned has no significant effect on the simulation results carried out with the MRF approach.

Performance comparison with and without the presence of the arm

In Figure 7 and Figure 8, the pressure contours for two different rotor phases (0° and 90° degrees of rotation) with and without the presence of the small distance square arm with respect to the center of the arm are depicted.

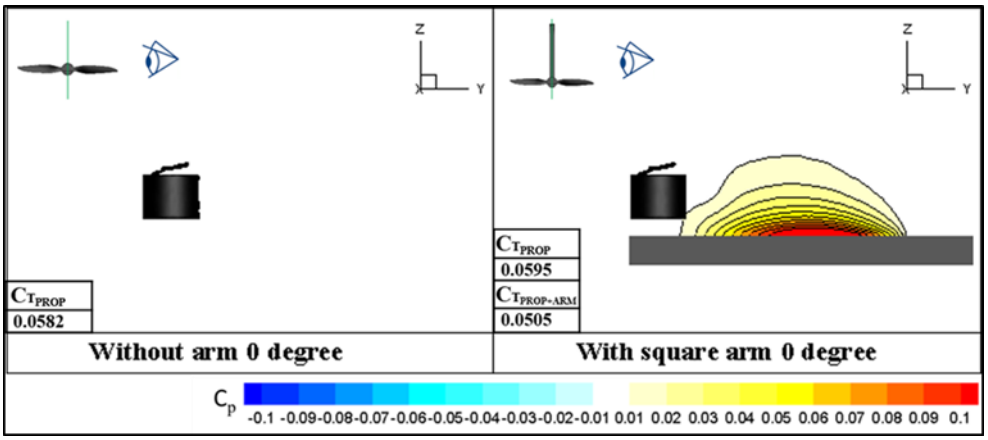

Figure 7. Pressure contours with and without the presence of the small distance square arm with respect to the center of the arm at the 0° rotor phase

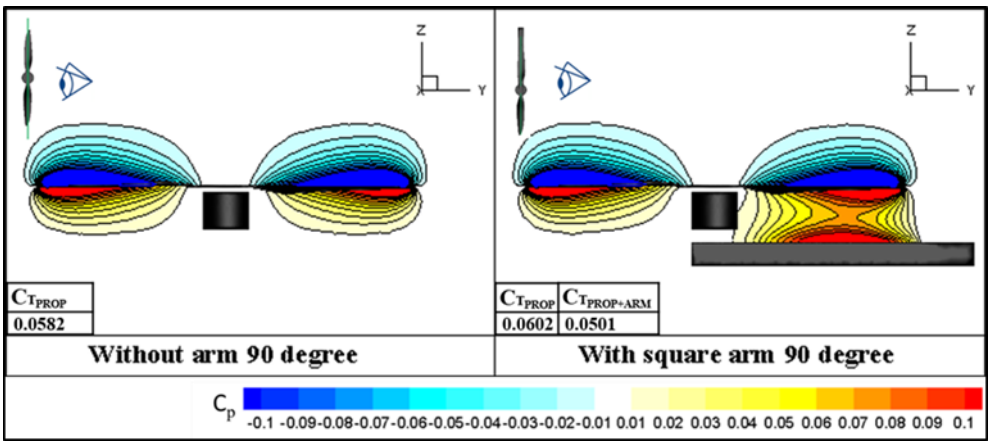

Figure 8. Pressure contours with and without the presence of the small distance square arm with respect to the center of the arm at the 90° rotor phase

There is a high-pressure zone when the arm is present compared to the without arm case in all phases which results in negative thrust in the downward direction leading to a decrease in the total rotor-arm thrust. However, this high-pressure zone increases the thrust generated by the propeller. The interaction between the rotor and the rotor affects the aerodynamic performance of the propeller in a way analogous to ground effect.

Effect of the different rotor frame arm shapes

In order to have a proper configuration to achieve a lower negative arm thrust following a greater total thrust; four different arm shapes are investigated. Small distance rotor frame-arm configuration performance comparison between the four different rotor frame-arm will be described in this section.

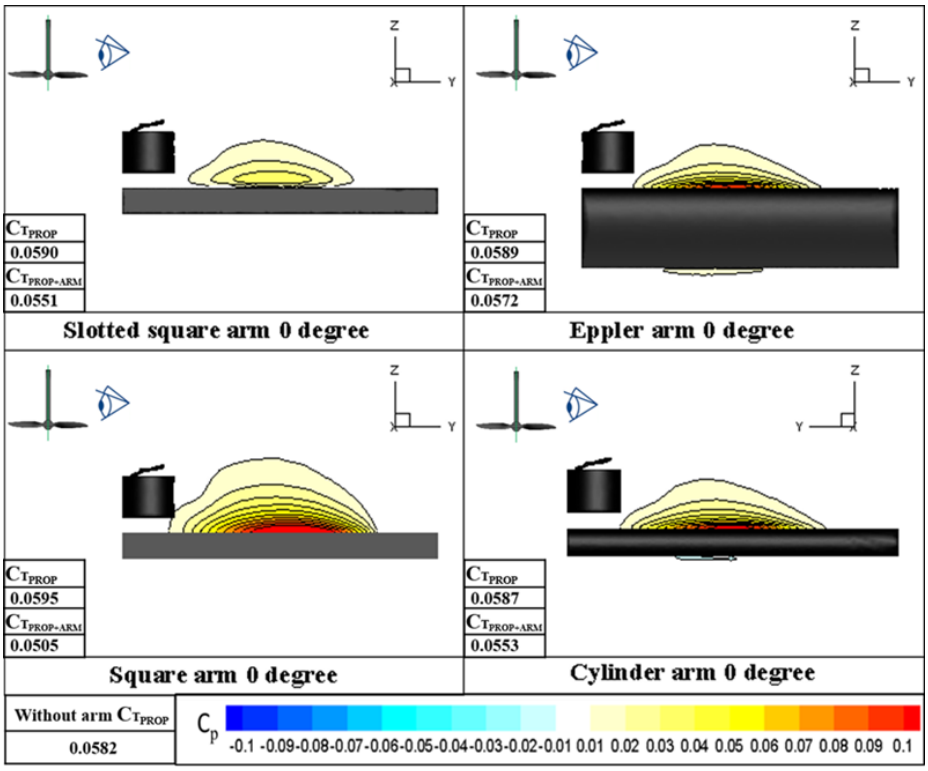

Figure 9. Pressure contours of the four different arms with respect to the center of the arm at the 0° rotor phase

In Figure 9, the pressure contours with the presence of square, slotted square, Eppler and cylindrical arm are shown with respect to the center of the arm at the 0° rotor phase. In all cases, there is a high-pressure zone when the arm is available producing a downward negative arm thrust. This follows with a decrease in total rotor-arm thrust compared to the without arm case. This positive pressure region is stronger in the case of the square arm, which also yields a higher propeller thrust due to increased pressure level at the pressure side of the propeller. However, this increased positive pressure region also increases the negative thrust (viz. drag) of the propeller arm and as a result, a small total thrust coefficient is obtained (see Table 2) In the table, C_{Tprop} stands for the thrust coefficient generated by the propeller only, whereas $C_{Tprop+arm}$ is the total thrust coefficient of the propeller-arm structure. In accordance with the aforementioned statement regarding the analogous ground effect, the decrease in the solidity of the propeller arm (i.e. slotted arm geometry) results in a decrease in the thrust coefficient of the propeller. However, arm-generated-drag also decreases and as a result a higher total thrust coefficient than the square arm geometry is achieved with the slotted arm.

Table 2. Thrust coefficient and Efficiency values of different rotor arm shapes

	Without Arm	Cylinder Arm	Eppler Arm	Square Arm	Slotted Square Arm
C_{Tprop}	0.0581	0.0588	0.0588	0.0596	0.0585
η_{prop}	0.3866	0.3902	0.3905	0.3960	0.3930
$C_{Tprop+arm}$	-	0.0554	0.0571	0.0503	0.0548
$\eta_{prop+arm}$	-	0.3564	0.3738	0.3074	0.3554

Small distance rotor frame-arm configuration performance analysis shows that by adding an arm to the simulation domain, the thrust of the propeller will be decreased. Among the different arm shapes, Eppler arm has the highest thrust coefficient value and total efficiency. Thus, the Eppler arm is the optimum arm shape among these four different arms. The average thrust coefficient and efficiency values for different arm shapes are shown in Table 2. In the table, $C_{T_{prop}}$ stands for the thrust coefficient generated by the propeller only, whereas $C_{T_{prop+arm}}$ is the total thrust coefficient of the propeller-arm structure.

The results of this study show that the propeller-Eppler arm configuration has 4.89%, 21.59%, and 5.18% greater propeller efficiency than that of the propeller-cylindrical arm, propeller-square arm, and propeller-slotted square arm configurations, respectively. For average total thrust values in all four different arms, the Eppler arm produces the minimum negative thrust following with the highest total thrust compared to three other cases. On the other hand, the thrust coefficient generated by the propeller only case ($C_{T_{prop}}$), the square arm geometry scores the best.

Rotor frame arm distance effects

For small distance rotor frame-arm configuration, the Eppler arm was shown to have the best performance among four different cases. In order to analyze the effect of rotor frame-arm distance on the rotor performance, two more cases for Eppler and slotted square arm configurations are considered at which in the middle-distance case, the distance between the rotor and arm is considered as 35 mm (20 mm shifted from the initial case), and in the long-distance case, the distance between the rotor and arm is considered as 55 mm (40 mm shifted from the initial case). The sketch of the initial (short) distance case is depicted in Figure 10.

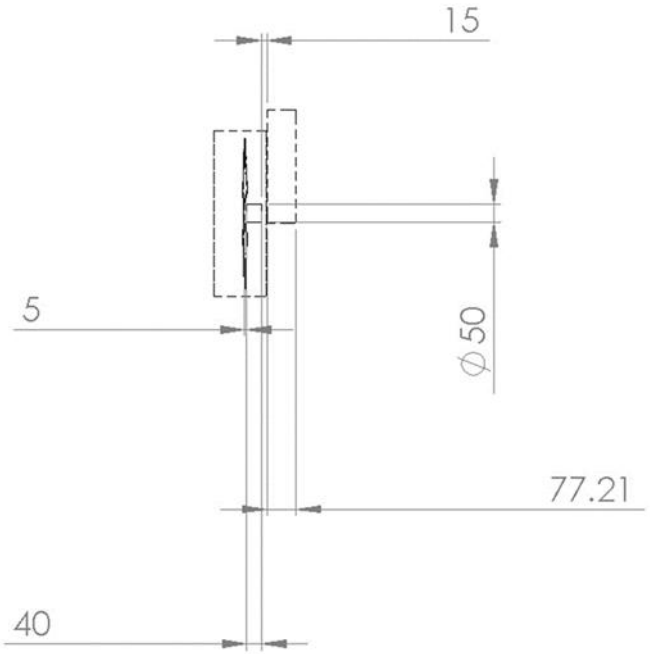

Figure 10: A sketch of small rotor frame-arm distance configuration in mm

Pressure contours of the small, middle, and long-distance rotor frame-arm configurations for Eppler and slotted rotor frame-arms are depicted in Figure 11. Although the presence of solid surfaces increases the thrust generation of the propeller, the negative thrust caused by the high-pressure region above the arm decreases the overall thrust of the arm structure. As seen in Figure 11, this interaction effect decreases with increasing arm distance. The average thrust coefficient and efficiency values for Eppler and Slotted square arm shown in Table 3.

Table 3. Thrust coefficient and Efficiency values for Eppler and Slotted square arm at the different rotor arm distances

Arm Type	C_{Tprop}	η_{prop}	$C_{Tprop+arm}$	$\eta_{prop+arm}$
Eppler Arm	0.0588	0.3905	0.0571	0.3738
Eppler Arm (+20mm)	0.0585	0.3893	0.0581	0.3849
Eppler Arm (+40mm)	0.0584	0.3889	0.0581	0.3851
Slotted Sq Arm	0.0585	0.3930	0.0548	0.3554
Slotted Sq. Arm (+20mm)	0.0586	0.3900	0.0570	0.3747
Slotted Sq. Arm (+40mm)	0.0585	0.3892	0.0571	0.3755

Averaged $C_{Tprop+arm}$ and $\eta_{prop+arm}$ results show that middle and long-distance Eppler arm geometries are more efficient than the small-distance Eppler and slotted square arm shapes. On the other hand, the average thrust coefficient formed by the middle and long-distance arms scores similarly. This situation shows that, after the middle-distance arm distance, the negative thrust in downward direction leading to a decrease in total rotor-arm thrust diminishes.

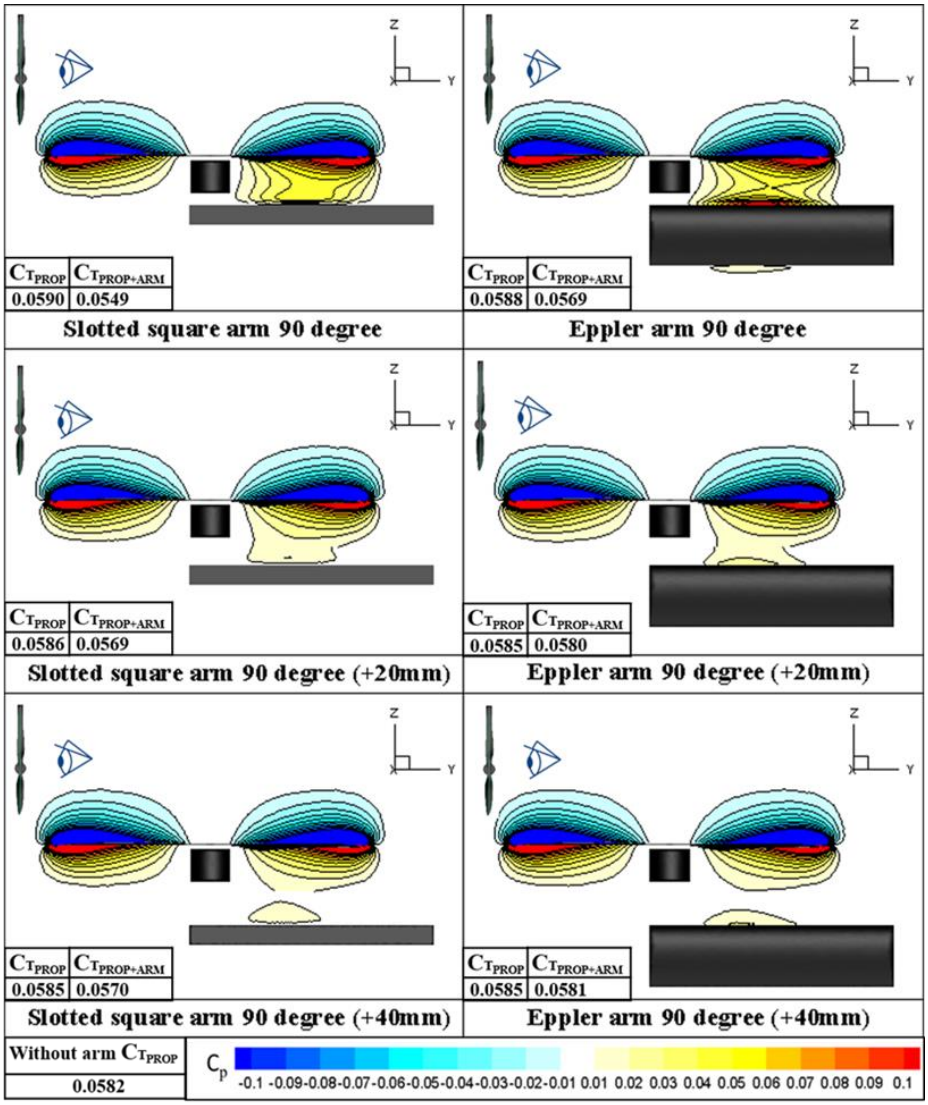

Figure 11. The pressure contour of the slotted square and Eppler arm with respect to the center of the arm for the small rotor frame-arm distance

CONCLUSIONS

This study numerically investigates the interaction between rotor and rotor frame-arm of different geometries in hovering flight by utilizing the commercially available computational fluid dynamics (CFD) solver software ANSYS Inc. Fluent 17. Therefore, four different rotor frame-arm configurations, (i.e., Eppler Arm, 25mm cylindrical tube, 25mm square tube, and 25mm square tube with a 10mm slot) are generated and investigated.

Two different propellers, APC Slow Flyer 11x4.7 propeller, and 16x4 carbon fiber propeller were used in this study. The thrust and torque measurements captured by using a loadcell with these propellers in the test section of the low-speed METUWIND C3 wind tunnel at the Rüzgem (Metuwind). In order to validate the experimental setup of used in this study, the APC Slow Flyer 11x4.7 propeller was utilized for propeller measurements comparison between the current data and measurements taken by Brandt [6]. The computational study phase of this study was carried out by using the 3D scanned version of a 16x4 carbon fiber propeller. Reynolds-Averaged Navier-Stokes simulations were performed by implementing the k-ω turbulence model. The numerical simulations were validated for hovering and vertical climb flight conditions with the thrust and torque measurement results of the 16x4 carbon fiber propeller at the various rotational speeds. Hovering flight performance simulations were conducted at 1050, 2000, and 3150 rpm values. Vertical climb flight performance simulations were performed at 2000 and 3150 rpm values by adjusting the flow domain speed to 3.42 and 5.42 m/s. Rotational speeds of the 16-inch propeller were set using the MRF approach.
As a result of the hovering flight CFD comparison study, when compared with the relevant test data, a maximum discrepancy of 10.44% for thrust and 7.28% for torque were obtained. For vertical climb flight, a maximum disparity of 10.81% for the thrust coefficient and 4.06% for the power coefficient was obtained. These results have proven that the applied CFD method is reliable for other similar CFD studies.

After validating numerical simulations, four different arm geometries added to the validated CFD model to assess their effect on the aerodynamic performance of the rotors. Arm structure study simulations were conducted using the MRF approach at 3150 rpm and hovering flight conditions. It was found that all arm geometries have a negative effect on the aerodynamic performance when compared to the without arm configuration. This negative effect is prominent, especially for the 25mm square tube arm. Overall, the Eppler arm geometry configuration gives the best performance at hovering flight.

The results of this study show that the propeller-Eppler arm configuration has 4.89%, 21.59%, and 5.18% greater propeller efficiency than that of the propeller-cylindrical arm, propeller-square arm, and propeller-slotted square arm configurations, respectively.
In all cases, the presence of solid surfaces increases the thrust generation of the propeller, the negative thrust caused by the high-pressure region above the arm decreases the overall thrust of the arm structure. This positive pressure region is stronger in the case of the square arm, which also yields a higher propeller thrust due to increased pressure level at the pressure side of the propeller.

References

Brandt, J. B., & Selig, M. S. (2011). Propeller Performance Data at Low Reynolds Numbers. *49th AIAA Aerospace Sciences Meeting*. https://doi.org/10.2514/6.2011-1255

Deters, R. W., Ananda, G. K., & Selig, M. S. (2014). Reynolds Number Effects on the Performance of Small-Scale Propellers. In *32nd AIAA Applied Aerodynamics Conference* (pp. 1–43). https://doi.org/10.2514/6.2014-2151

Eppler, R. (1990). *Airfoil Design and Data*. Berlin, Heidelberg: Springer Berlin Heidelberg. https://doi.org/10.1007/978-3-662-02646-5

Kaya, D. D. (2014). *Modeling and Experimental Identification of Quadrotor Aerodynamics*. Retrieved from http://etd.lib.metu.edu.tr/upload/12617982/index.pdf

Kutty, H. A., Rajendran, P., & Mule, A. (2017). Performance analysis of small scale UAV propeller with slotted design. *2017 2nd International Conference for Convergence in Technology, I2CT 2017*. https://doi.org/10.1109/I2CT.2017.8226219

Penkov, I., & Aleksandrov, D. (2017). Analysis and study of the influence of the geometrical parameters of mini unmanned quad-rotor helicopters to optimise energy saving. *International Journal of Automotive and Mechanical Engineering*. https://doi.org/10.15282/ijame.14.4.2017.11.0372

Stajuda, M., Karczewski, M., Obidowski, D., & Krzysztof, J. (2016). Development of a CFD Model for Propeller simulation. *Mechanics and Mechanical Engineering*, *20*(4), 579–593. https://doi.org/10.13140/RG.2.1.3154.4406

Theys, B., Dimitriadis, G., Hendrick, P., & Schutter, J. De. (2016). Influence of propeller configuration on propulsion system efficiency of multi-rotor Unmanned Aerial Vehicles, (June). https://doi.org/10.1109/ICUAS.2016.7502520